

# High-Speed Modulator Based on Electro-Optic Polymer Infiltrated Subwavelength Grating Waveguide Ring Resonator

Zeyu Pan, Xiaochuan Xu,\* Chi-Jui Chung, Hamed Dalir, Hai Yan, Ke Chen, Yaguo Wang, Baohua Jia, and Ray T. Chen\*

Silicon-organic hybrid integrated devices show great potential in high-speed optical interconnects and sensors. In this paper, a high-speed modulator based on an electro-optic (EO) polymer (SEO125) infiltrated sub-wavelength grating (SWG) waveguide ring resonator is presented. The core of the SWG waveguide consists of periodically arranged silicon pillars along the light propagation direction, which provides large mode volume overlap with EO polymer. The optimized SWG shows a mode volume overlap of 36.2% with a silicon duty cycle of 0.7. The 3-dB modulation bandwidth of the fabricated modulator is measured to be larger than 40 GHz occupying an area of  $70\ \mu\text{m} \times 29\ \mu\text{m}$ , which is the largest bandwidth and the most compact footprint that has been demonstrated for ring resonators on the silicon-organic hybrid platform.

## 1. Introduction

Silicon photonics<sup>[1,2]</sup> has been widely accepted as one of the essential technologies in the next generation optical interconnect.<sup>[3–5]</sup> One of the intrinsic obstacles is the absence of  $\chi^{(2)}$ -nonlinearity in unstrained silicon due to its centrosymmetric crystal structure, making modulating photons on silicon platform a great challenge. State-of-the-art silicon photonic modulators rely on plasma dispersion,<sup>[6–8]</sup> which modulates both the real and imaginary components of the refractive index,


causing undesired nonlinear response.<sup>[9,10]</sup> Although more than 50 Gbits<sup>−1</sup> on-off keying has been demonstrated with reverse-biased p-n junctions,<sup>[11]</sup> achieving a small footprint, low power consumption, low modulation voltage and high-speed modulator is still challenging.<sup>[12]</sup>

The silicon-organic hybrid (SOH) platform enables the marriage of the best of the two materials and thus has been receiving substantial attention. Compared to plasma dispersion,<sup>[13]</sup> electro-optic (EO) polymers have a remarkable EO coefficient ( $r_{33} > 400\text{pm/V}$ ),<sup>[14]</sup> ultrafast response speed ( $< 1\text{fs}$ ),<sup>[15–17]</sup> small dispersion, and spin-casting compatibility, which promise low-power consumption,

ultra-high speed modulation, and ease of fabrication.<sup>[4]</sup> Modulators with bandwidth over 100 GHz have been demonstrated,<sup>[12,18]</sup> but their millimeter long device length defeats the purpose of chip-scale integration.<sup>[19–21]</sup> Structural slow light, such as slot photonic crystals<sup>[22,23]</sup> and plasmonic devices,<sup>[24,25]</sup> can effectively shrink the phase shifter size but at the price of significantly increased insertion loss.<sup>[26–30]</sup> Inspired by the success of silicon microring resonators, a few attempts have been made to replicate microrings on SOH platform<sup>[31]</sup> through several waveguiding structures.<sup>[32–38]</sup> Strip waveguides based microring resonators with EO polymer as top cladding have a radius of  $40\ \mu\text{m}$ .<sup>[32,39]</sup> The performance of the devices is limited by the small overlap between EO polymer and the guided mode.<sup>[32,39]</sup> Slot waveguide based ring resonators can increase the mode volume overlap significantly but suffer from an ultra-high loss of 35 dB/cm.<sup>[31,40]</sup> The diameter of the slot waveguide based ring resonator is as large as  $60\ \mu\text{m}$ .<sup>[31]</sup>

In this paper, we report a subwavelength grating (SWG) ring resonator based modulator. Compared to slot waveguides, SWG provides competitive mode volume overlap and a comparable propagation loss as strip waveguides.<sup>[41]</sup> A 3-dB small signal modulation bandwidth larger than 40 GHz has been observed, occupying merely an area of  $70\ \mu\text{m} \times 29\ \mu\text{m}$ . According to the authors' best knowledge, it is the most compact and fastest ring resonator modulator that has been demonstrated on the SOH platform.

Dr. Z. Pan, Dr. X. Xu, C.-J. Chung, Dr. H. Yan, Prof. R. T. Chen  
Department of Electrical and Computer Engineering  
The University of Texas at Austin  
10100 Burnet Rd, MER 160, Austin, TX 78758, USA  
E-mail: xiaochuan.xu@omegapoptics.com; chenrt@austin.utexas.edu  
Dr. X. Xu, Dr. H. Dalir, Prof. R. T. Chen  
Omega Optics Inc.  
8500 Shoal Creek Blvd, Austin, TX, 78757, USA  
Dr. K. Chen, Prof. Y. Wang  
Department of Mechanical Engineering  
The University of Texas at Austin  
Austin, TX 78712, USA  
Prof. B. Jia  
Centre for Micro-Photonics  
Swinburne University of Technology  
John Street, Hawthorn, Victoria 3122, Australia

 The ORCID identification number(s) for the author(s) of this article can be found under <https://doi.org/10.1002/lpor.201700300>

DOI: 10.1002/lpor.201700300

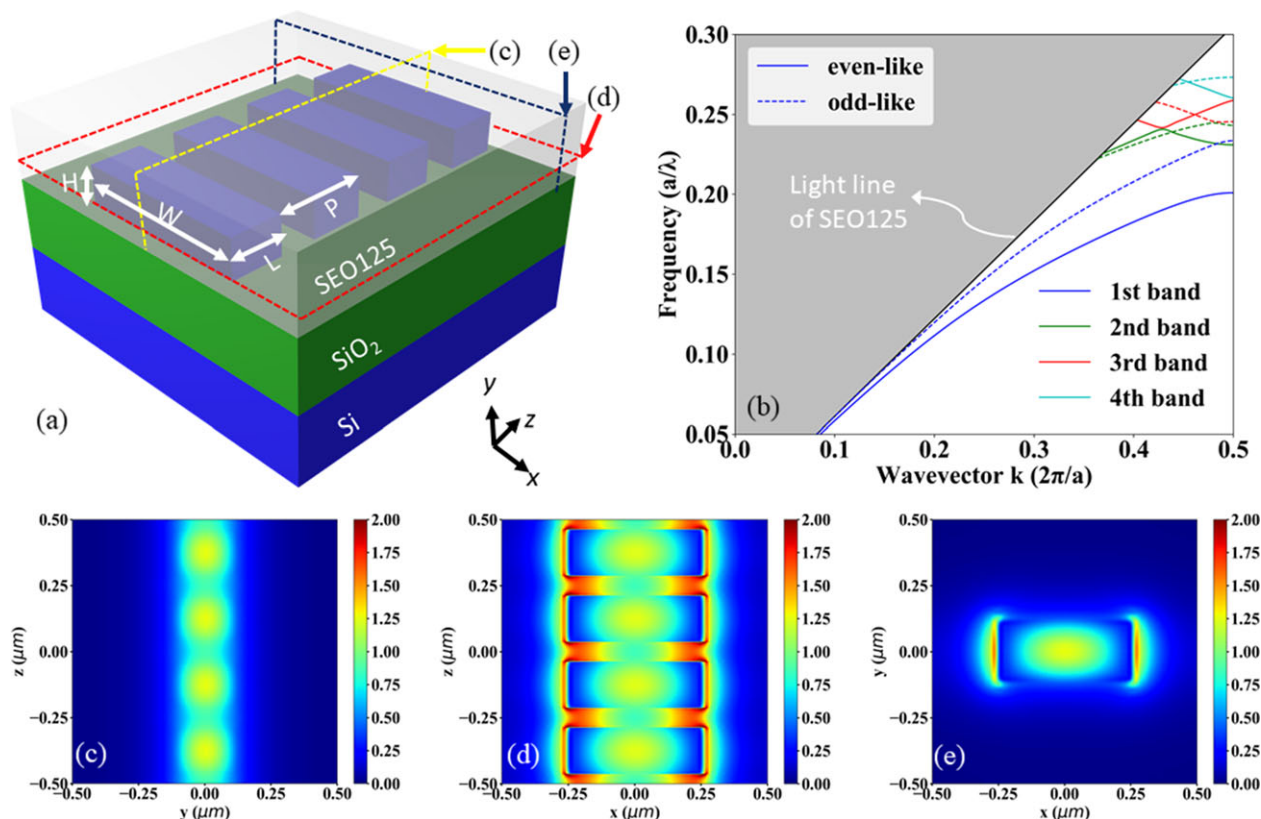


**Figure 1.** a) Schematic of an SWG waveguide for the optical modulator. b) Photonic band structure of SWG waveguides with SEO125 as top cladding for the waveguide width  $W = 500$  nm and pillar length  $L = 175$  nm. The black line at the boundary of the grey region indicates the light line of SEO125. The solid and dashed lines indicate the even-like and odd-like modes respect to the central slab plane in the  $y$ -direction, respectively. The electrical field distribution of the SWG waveguide at c)  $x$ -slice ( $x = 0$   $\mu\text{m}$ ), d)  $y$ -slice ( $y = 0$   $\mu\text{m}$ ), and e)  $z$ -slice ( $z = 0$   $\mu\text{m}$ ), for the SWG waveguide width  $W = 500$  nm, pillar length  $L = 175$  nm, height  $H = 220$  nm, and period  $P = 250$  nm.

## 2. Experimental Section

The schematic of SWG waveguides<sup>[42–49]</sup> is shown in **Figure 1a**. The hybrid waveguide core is formed by periodically interlacing segments of high and low refractive index materials at a subwavelength pitch. The top and bottom claddings are EO polymer SEO125 (Soluxra LLC) and silicon dioxide, respectively. SEO125 is stable at a temperature below 90 °C. The optical mode propagates along the  $z$ -direction and its optical properties can be tuned by adjusting the period ( $P$ ), waveguide width ( $W$ ), pillar length ( $L$ ), and Si thickness ( $H$ ). The simulated photonic band structure of the SEO125/silicon SWG waveguides, using the 3D plane wave expansion method (RSoft, inc.), is shown in **Figure 1b**. The black line represents the light line of SEO125 ( $n = 1.63$ ). The solid and dashed lines denote even- and odd-like modes, respectively, which are categorized according to their modes with respect to the central slab plane in the  $y$ -direction. When the modes are away from the edge of reduced Brillouin zone, the dispersion characteristic of the guided modes resembles that of a uniform waveguide. The electrical fields  $|E_x|^2$  of optical modes, which is aligned parallel to the poling direction of SEO125, at  $x$ -slice ( $x = 0$   $\mu\text{m}$ ),  $y$ -slice ( $y = 0$   $\mu\text{m}$ ), and  $z$ -slice ( $z = 0$   $\mu\text{m}$ ) are plotted in **Figure 1c–e**, respectively. It can be observed that there is a strong optical field exists outside Si

pillars in the SEO125 region. The mode volume overlap integral  $f = \int_{\text{SEO125}} \epsilon |E_x|^2 dv / \int_{\text{total}} \epsilon |E_x|^2 dv$  is adopted to quantify the optical field in SEO125. We analyzed the mode volume overlap factor  $f$ , effective index, and group index of the SWG waveguides versus the duty cycle ( $= L/P$ ), the waveguide width  $W$ , and SWG period ( $P$ ), as shown in Supporting Information **Figures S1 and S2**. As SWG duty cycle, the waveguide width  $W$ , or SWG period decreases, mode volume overlap factor  $f$  increases, meaning that more electrical energy is concentrated inside SEO125 region. It can also be seen that the period does not affect the SWG much, if the subwavelength condition ( $p < \lambda/4$ ) is satisfied, where  $\lambda$  is the wavelength inside the waveguide. In this paper, SWG is optimized to operate at  $\lambda_0 = 1565$  nm, and we will focus on the fundamental TE-like mode (blue solid line in **Figure 1b**). To ensure the SWG structure operates in the subwavelength regime and ease of fabrication, we choose the period  $P = 250$  nm, and the pillar length  $L = 175$  nm, corresponding to a duty cycle of 0.7, along with the waveguide width  $W = 500$  nm. In this configuration, the mode volume overlap integral  $f$  equals 36.2%. Compared a typical strip waveguide ( $f \approx 4.0\%$ ), it increases around 9 times.

The proposed SWG ring resonator based modulator is shown in **Figure 2a**. Subwavelength grating couplers are exploited for interfacing single mode fibers.<sup>[50,51]</sup> The rounded rectangular shape is adopted instead of the most common circular shape to gain

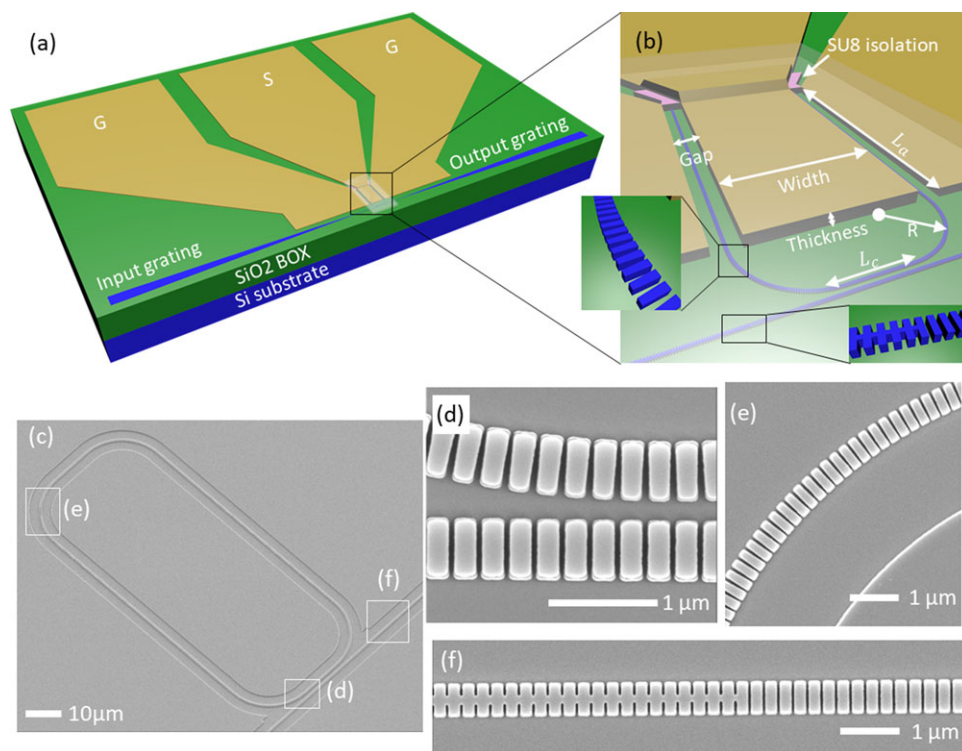


**Figure 2.** a) Schematic of an EO polymer modulator based on the SWG ring resonator. The device is fabricated on a silicon-on-insulator (SOI) wafer. The input and output grating couplers are used to couple the light into and out of the device, respectively. The “G”, “S”, and “G” electrode pads are used to connect with a GSG high-speed RF probe, which is used to provide the RF signal to modulate the EO polymer modulator based on the SWG ring resonator. b) The zoomed-in schematic of the SWG ring resonator. SWG is used for both the ring and the bus waveguide. The trapezoid SWG is used at the SWG bends to reduce the bending loss. A converter is used to convert between the conventional strip mode and SWG mode. SU-8 island is used to isolate the center electrode and ring resonator. The transparent region in (a) and (b) indicates the coated EO polymer. c) SEM images of the fabricated SWG ring resonator and d–f) zoomed in images.

more flexibility in tuning the coupling strength between the bus waveguide and the ring resonator. The zoomed-in schematic of the SWG ring resonator is shown in Figure 2b. The shape of the ring resonator is defined by the coupling length  $L_c$ , phase shifter length  $L_a$ , and bending radius  $R$ , which are 9  $\mu\text{m}$ , 50  $\mu\text{m}$ , and 10  $\mu\text{m}$ , respectively. The SWG ring resonator is formed by the SWG waveguide<sup>[46,49]</sup> optimized in the previous paragraph except for the four bends at the corners, in which trapezoidal shape pillars are fine-tuned to minimize the bending loss.<sup>[52,53]</sup> SU-8 island is used to isolate the center electrode and ring resonator. The  $n_{\text{eff}}$  of the SWG waveguide with SEO125 and SU8 cladding is 2.031 and 1.994, respectively. The reflection between two waveguides is merely 0.0085%. Thus, the influence of using SU-8 island can be ignored. Due to the compact size, the walk-off between electrical and optical signal is negligible. Thus, high-speed modulation can be readily achieved with lumped electrodes.<sup>[54]</sup> It has been proved that without 50  $\Omega$  termination, lumped electrodes can effectively reduce the power consumption compared to traveling wave electrodes.<sup>[55,56]</sup> To reduce the reflection of RF signals, ground-signal-ground (GSG) electrodes are designed and optimized with Ansys HFSS to provide 50  $\Omega$  impedance match with GSG RF probes. As shown in Figure 2b, the central width, gold thickness, and gap are 25  $\mu\text{m}$ , 2.4  $\mu\text{m}$ , and 4  $\mu\text{m}$  respectively. The detailed simulation process can be found in Supporting Information Figure S4.

The modulator is fabricated on a silicon-on-insulator (SOI) chip. The SWG ring resonator is patterned by e-beam lithography and reactive ion etching (RIE). A 2.6  $\mu\text{m}$  thick SU-8 island is formed by photolithography to let the electrodes cross over the SWG waveguide without causing any optical loss. Then the electrodes are fabricated with the standard liftoff process. Finally, EO polymer is spin-casted and cured under 80  $^{\circ}\text{C}$  for 5 hours in the vacuum oven to assure the entire subwavelength structures are infiltrated. The detailed fabrication procedure can be found in Supporting Information Figure S5. The SEM of the fabricated SWG ring resonator is shown in Figure 2c–f.

### 3. Results and Discussion

The transmission of the fabricated SWG ring resonator is characterized by amplified spontaneous emission (ASE) broadband optical source and optical spectrum analyzer (OSA).<sup>[50,51]</sup> To maximize the extinction ratio, a set of devices with different gaps are fabricated and measured. The spectra are summarized in Figure 3a. The relation between the extinction ratio and the gap is extracted and plotted in Figure 3b. The maximum extinction ratio is  $25.9 \pm 3.5$  dB, corresponding to an edge-to-edge gap of 500 nm between the bus waveguide and the ring resonator. The on-chip insertion loss of the modulator is around 4 dB.



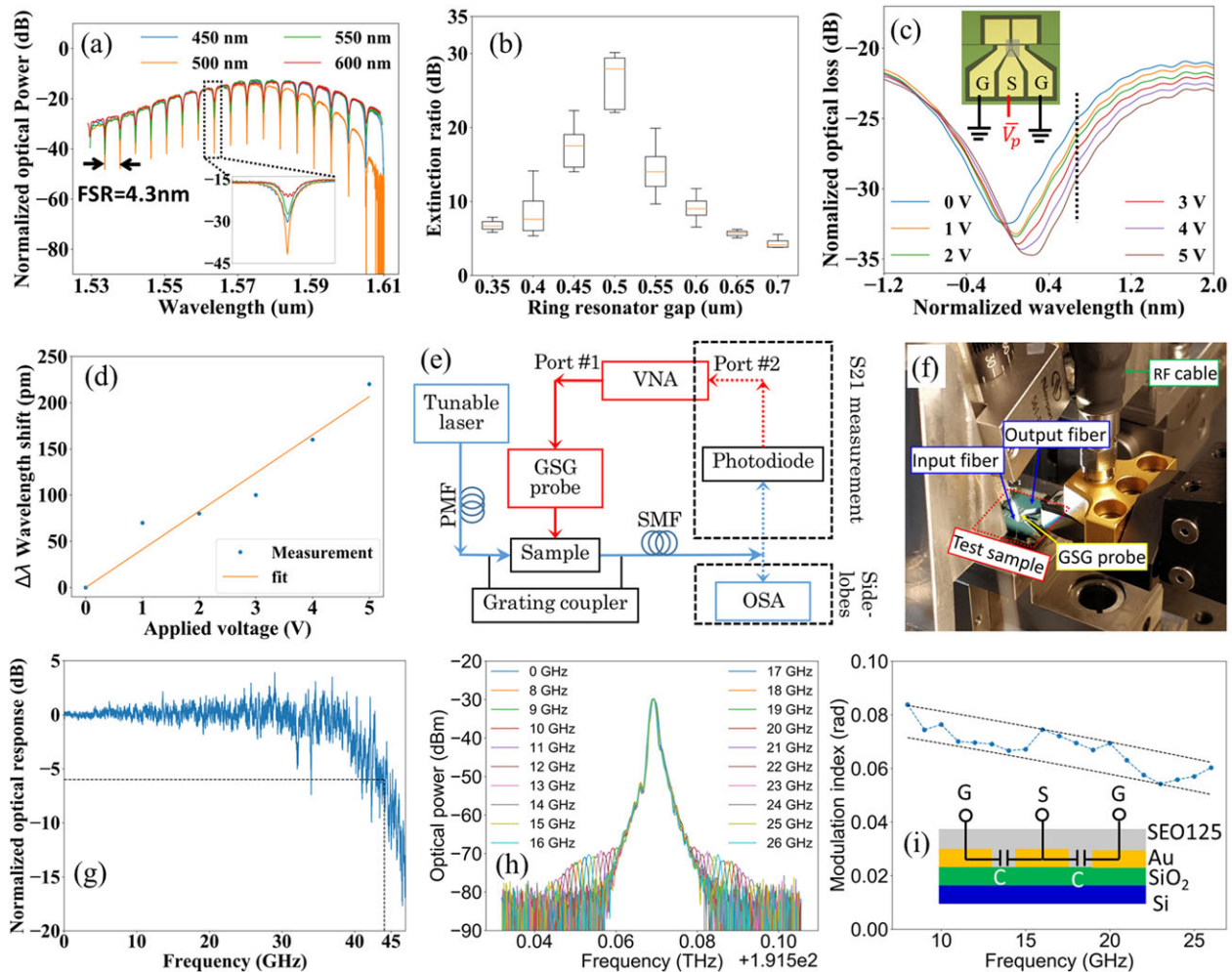


**Figure 3.** a) The normalized optical spectrums with the gap size 450 nm, 500 nm, 550 nm and 600 nm. b) The measured extinction ratio versus the gap size between the bus and the ring. c) The spectrum resonance shift after applied the electric field. The DC voltage is applied to the electrodes with a configuration in the insert. d) The wavelength shift in picometer versus the applied electrical voltage. e) The setup to measure the RF response and side-lobe of the modulator. The blue and red lines indicate the optical and RF signal, respectively. The top and bottom dashed boxes are used to measure the S21 response and side-lobes, respectively. f) The magnified view of the sample connected with fibers using the grating coupler and RF cables using the GSG probe. g) The measured and normalized optical response versus the frequency. h) The measured optical transmission spectra of the modulator operating at 8–26 GHz. i) The modulation index versus frequency. The modulation index results are normalized to a 10 dBm launched power. The equivalent circuit of the modulator is shown in the insert.

The EO-polymer is poled at 150 °C for 1 minute to align the chromophore molecules, and then the temperature slowly reduces to the room temperature. The extinction ratio decreases drastically to  $\approx 10$  dB due to the scattering centers formed by non-uniform refractive index of the EO-polymer induced during poling.<sup>[57–59]</sup> To characterize the poling efficiency, DC voltage is applied to the electrodes with a configuration shown in the inset of Figure 3c. The red shift of the resonance is observed and plotted in Figure 3c. The resonance shift versus the applied voltage is summarized in Figure 3d. The orange solid line is the linear fitting of the measurement data, giving an averaged resonance shift of 41.3 pm/V. Thus, from the electro-optic effect  $\Delta n = \frac{1}{2} r_{33} n^3 \frac{V}{d}$ ,<sup>[60]</sup> the EO coefficient is estimated to  $r_{33} = 54.7$  pm/V, corresponding to a poling efficiency of 43.8% compared to the EO coefficient of the bulk EO polymer. The wavelength

dependence of the EO coefficient  $r_{33}$  is very small at the telecommunication wavelength.<sup>[61,62]</sup>

The setup to measure the optical response and side-lobe of the modulator is shown in Figure 3e. The blue and red lines indicate the optical and RF signal, respectively. The top and bottom dashed boxes are used to measure the S21 response and side-lobes, respectively. The single wavelength light is generated by a tunable laser (Santec ECL200). A polarization maintaining fiber (PMF, OZ Optics PMF-1550-8/125-0.25-L) is used to couple the light into the modulator. The light from the output grating coupler is collected by a standard single mode fiber (SMF, Corning SMF-28).<sup>[50,51]</sup> The RF signal, which is output from the port #1 of the vector network analyzer (VNA, Agilent N5230A), is applied to the sample via a GSG probe (Cascade ACP40-GSG-250). The aligned grating couplers and the applied GSG probe is shown in

Figure 3f. For the S21 response measurement, a high-speed photodiode (New Focus 1014 45-GHz) converts the optical signal into the RF signal, which is fed into the port #2 of the VNA. For the side-lobe measurement, the output optical signal from SMF is directly connected to the optical spectrum analyzer (OSA, ANDO AQ6317B).

The measured and normalized optical response of the SWG optical modulator is shown in Figure 3g. The optical response is measured at the rising edge of the resonance, which is the black dashed line in Figure 3c. The reflection from port #1 is subtracted during normalization. The measured 3-dB bandwidth is  $41.4 \pm 1.1$  GHz, and the 6-dB bandwidth is  $44.1 \pm 1.6$  GHz. The measured optical transmission spectra of the modulator operating at 8–26 GHz, as shown in Figure 3h. The modulation index versus frequency is shown in Figure 3i. The modulation index results are normalized to a 10 dBm launch power. The observed small signal bandwidth is limited by our measurement instruments (e.g. 2.92mm RF cables have a 3-dB bandwidth of 40 GHz). The potential bandwidth can be estimated by  $\frac{1}{f_c^2} = \frac{1}{f_p^2} + \frac{1}{f_{RC}^2}$ , where  $f_p$  and  $f_{RC}$  denote the photon lifetime and RC delay determined cutoff frequencies, respectively.<sup>[63]</sup> Since the  $Q$  factor of the resonator is  $\approx 1000$  after poling, corresponding to a photon lifetime of  $\approx 0.83$  ps, the photon lifetime induced cut-off frequency  $f_p = \frac{1}{2\pi\tau_p} = 192$  GHz. The equivalent circuit of the modulator is shown in the inset of Figure 3i. As the modulator is directly driven by the electric field between the gold electrodes with negligible resistance,  $f_{RC}$  is infinite. The cutoff frequency is mainly limited by the photon lifetime, which potentially could offer a frequency response of up to 192 GHz.<sup>[63]</sup>

As aforementioned, due to the compact device footprint, lumped electrodes without termination are used to apply electrical signals. The power consumption is equivalent to charging and discharging two capacitors. The total capacitance<sup>[33]</sup> is estimated to be 0.4 fF. According to Figure 3c, assuming  $V_{pp} = 5.0$  V is selected, which corresponds to a 6 dB on-off ratio, the power consumption can be estimated by  $\frac{1}{4}CV^2 = 2.5$  fJ/bit, assuming equal probabilities of logical ones and zeros and only transitions consume energy. The power consumption can be further improved by reducing the capacity, which can be readily achieved by reducing the size of the ring.

## 4. Conclusion

We have demonstrated a high-speed optical modulator based on electro-optic polymer infiltrated subwavelength grating waveguide ring resonator. Compared to a conventional strip waveguide, SWG structure increases the interactive volume between the optical signal and EO polymer. The measured 3-dB bandwidth is larger than 40 GHz. The power consumption for digital communication is 2.6 fJ/bit. The bandwidth can be further increased and the power consumption can be further decreased by reducing the duty cycle or the size of the ring resonator.

## Supporting Information

Supporting Information is available from the Wiley Online Library or from the author.

## Acknowledgements

Z.P. and X.X. equally contributed for this work. This research is supported by Department of Energy (DOE) under the contract # DE SC-0013178 and Air Force Office of Scientific Research (AFOSR) Small Business Innovation Research (SBIR) under the contract # FA9550-16-C-0033.

## Conflict of Interest

The authors declare no conflict of interest.

## Keywords

electro-optic polymers, optical modulators, ring resonators, silicon photonics, sub-wavelength grating

Received: November 9, 2017

Revised: March 20, 2018

Published online: May 17, 2018

- [1] R. A. Soref, *Proc. IEEE* **1993**, *81*, 1687.
- [2] R. Soref, *IEEE J. Sel. Top. Quantum Electron.* **2006**, *12*, 1678.
- [3] D. Thomson, A. Zilkie, J. E. Bowers, T. Komljenovic, G. T. Reed, L. Vivien, D. Marris-Morini, E. Cassan, L. Viro, J.-M. Fédéli, J.-M. Hartmann, J. H. Schmid, D.-X. Xu, F. Boeuf, P. O'Brien, G. Z. Mashanovich, M. Nedeljkovic, *J. Opt.* **2016**, *18*, 73003.
- [4] H. Subbaraman, Z. Pan, C. Zhang, Q. Li, L. J. Guo, R. T. Chen, in *Photonics West*, Vol. 9753, SPIE, **2016**, p. 97530Y–97530Y–10.
- [5] J. E. Bowers, T. Komljenovic, M. Davenport, J. Hulme, A. Y. Liu, C. T. Santis, A. Spott, S. Srinivasan, E. J. Stanton, C. Zhang, in *Photonics West*, Vol. 9774, SPIE, **2016**, p. 977402.
- [6] R. Ding, Y. Liu, Y. Ma, Y. Yang, Q. Li, A. E.-J. Lim, G.-Q. Lo, K. Bergman, T. Baehr-Jones, M. Hochberg, *J. Light. Technol.* **2014**, *32*, 2240.
- [7] R. Ding, Y. Liu, Q. Li, Y. Yang, Y. Ma, K. Padmaraju, A. E.-J. Lim, G.-Q. Lo, K. Bergman, T. Baehr-Jones, M. Hochberg, *Opt. Commun.* **2014**, *321*, 124.
- [8] H. Xu, X. Li, X. Xiao, Z. Li, Y. Yu, J. Yu, *IEEE J. Sel. Top. Quantum Electron.* **2014**, *20*, XX.
- [9] R. Soref, B. Bennett, *IEEE J. Quantum Electron.* **1987**, *23*, 123.
- [10] G. P. Agrawal, *Lightwave Technology: Components and Devices*, John Wiley & Sons, **2004**.
- [11] D. J. Thomson, F. Y. Gardes, J. M. Fedeli, S. Zlatanovic, Y. Hu, B. P. P. Kuo, E. Myslivets, N. Alic, S. Radic, G. Z. Mashanovich, G. T. Reed, *IEEE Photon. Technol. Lett.* **2012**, *24*, 234.
- [12] L. Alloatti, R. Palmer, S. Diebold, K. P. Pahl, B. Chen, R. Dinu, M. Fournier, J.-M. Fedeli, T. Zwick, W. Freude, C. Koos, J. Leuthold, *Light Sci. Appl.* **2014**, *3*, e173.
- [13] D. Perez-Galacho, C. Baudot, T. Hirtzlin, S. Messaoudène, N. Vulliet, P. Crozat, F. Boeuf, L. Vivien, D. Marris-Morini, *Opt. Express* **2017**, *25*, 11217.
- [14] W. Heni, C. Haffner, D. L. Elder, A. F. Tillack, Y. Fedoryshyn, R. Cottier, Y. Salamin, C. Hoessbacher, U. Koch, B. Cheng, B. Robinson, L. R. Dalton, J. Leuthold, *Opt. Express* **2017**, *25*, 2627.
- [15] B. Bortnik, Y.-C. Hung, H. Tazawa, B.-J. Seo, J. Luo, A. K.-Y. Jen, W. H. Steier, H. R. Fetterman, *IEEE J. Sel. Top. Quantum Electron.* **2007**, *13*, 104.
- [16] L. Gu, W. Jiang, X. Chen, R. T. Chen, *IEEE J. Sel. Top. Quantum Electron.* **2008**, *14*, 1132.
- [17] D. Chen, H. R. Fetterman, A. Chen, W. H. Steier, L. R. Dalton, W. Wang, Y. Shi, *Appl. Phys. Lett.* **1997**, *70*, 3335.

- [18] S. Koeber, R. Palmer, M. Lauermaun, W. Heni, D. L. Elder, D. Korn, M. Woessner, L. Alloatti, S. Koenig, P. C. Schindler, H. Yu, W. Bogaerts, L. R. Dalton, W. Freude, J. Leuthold, C. Koos, *Light Sci. Appl.* **2015**, 4, e255.
- [19] H. Zwickel, S. Wolf, C. Kieninger, Y. Kutuvantavida, M. Lauermaun, T. de Keulenaer, A. Vyncke, R. Vaernewyck, J. Luo, A. K.-Y. Jen, W. Freude, J. Bauwelinck, S. Randel, C. Koos, *Opt. Express* **2017**, 25, 23784.
- [20] C. Kieninger, Y. Kutuvantavida, H. Zwickel, S. Wolf, M. Lauermaun, D. Elder, L. Dalton, W. Freude, S. Randel, C. Koos, S. Randel, C. Koos, C. Koos, in *Conference on Lasers and Electro-Optics*, OSA, **2017**, p. STu3N.2.
- [21] H. Zwickel, T. De Keulenaer, S. Wolf, C. Kieninger, Y. Kutuvantavida, M. Lauermaun, M. Verplaetse, R. Pierco, R. Vaernewyck, A. Vyncke, X. Yin, G. Torfs, W. Freude, E. Mentovich, J. Bauwelinck, C. Koos, in *Optical Fiber Communications Conference and Exhibition*, OFC, **2017**.
- [22] J.-M. Brosi, C. Koos, L. C. Andreani, M. Waldow, J. Leuthold, W. Freude, *Opt. Express* **2008**, 16, 4177.
- [23] X. Zhang, C.-J. Chung, A. Hosseini, H. Subbaraman, J. Luo, A. K.-Y. Jen, R. L. Nelson, C. Y.-C. Lee, R. T. Chen, *J. Light. Technol.* **2016**, 34, 2941.
- [24] C. Koos, J. Leuthold, W. Freude, M. Kohl, L. Dalton, W. Bogaerts, A. L. Giesecke, M. Lauermaun, A. Melikyan, S. Koeber, S. Wolf, C. Weimann, S. Muehlbrandt, K. Koehnle, J. Pfeifle, W. Hartmann, Y. Kutuvantavida, S. Ummethala, R. Palmer, D. Korn, L. Alloatti, P. C. Schindler, D. L. Elder, T. Wahlbrink, J. Bolten, *J. Light. Technol.* **2016**, 34, 256.
- [25] A. Melikyan, L. Alloatti, A. Muslija, D. Hillerkuss, P. C. Schindler, J. Li, R. Palmer, D. Korn, S. Muehlbrandt, D. Van Thourhout, B. Chen, R. Dinu, M. Sommer, C. Koos, M. Kohl, W. Freude, J. Leuthold, *Nat. Photonics* **2014**, 8, 229.
- [26] H. Yan, X. Xu, C.-J. Chung, H. Subbaraman, Z. Pan, S. Chakravarty, R. T. Chen, *Opt. Lett.* **2016**, 41, 5466.
- [27] R. Palmer, S. Koeber, D. L. Elder, M. Woessner, W. Heni, D. Korn, M. Lauermaun, W. Bogaerts, L. Dalton, W. Freude, J. Leuthold, C. Koos, *J. Light. Technol.* **2014**, 32, 2726.
- [28] R. Palmer, L. Alloatti, D. Korn, P. C. Schindler, R. Schmogrow, W. Heni, S. Koenig, J. Bolten, T. Wahlbrink, M. Waldow, H. Yu, W. Bogaerts, P. Verheyen, G. Lepage, M. Pantouvaki, J. Van Campenhout, P. Absil, R. Dinu, W. Freude, C. Koos, J. Leuthold, *IEEE Photonics J.* **2013**, 5, 6600907.
- [29] R. Ding, T. Baehr-Jones, Y. Liu, R. Bojko, J. Witzens, S. Huang, J. Luo, S. Benight, P. Sullivan, J.-M. Fedeli, M. Fournier, L. Dalton, A. Jen, M. Hochberg, *Opt. Express* **2010**, 18, 15618.
- [30] T. Baehr-Jones, B. Penkov, J. Huang, P. Sullivan, J. Davies, J. Takayasu, J. Luo, T.-D. Kim, L. Dalton, A. Jen, M. Hochberg, A. Scherer, *Appl. Phys. Lett.* **2008**, 92, 163303.
- [31] M. Gould, T. Baehr-Jones, R. Ding, S. Huang, J. Luo, A. K.-Y. Jen, J.-M. Fedeli, M. Fournier, M. Hochberg, *Opt. Express* **2011**, 19, 3952.
- [32] J. Takayasu, M. Hochberg, T. Baehr-Jones, E. Chan, Guangxi Wang, P. Sullivan, Yi Liao, J. Davies, L. Dalton, A. Scherer, W. Krug, *J. Light. Technol.* **2009**, 27, 440.
- [33] X. Sun, D. Dai, L. Thylén, L. Wosinski, **2015**, 2, 1116.
- [34] P. Steglich, C. Mai, D. Stolarek, S. Lischke, S. Kupijai, C. Villringer, S. Pulwer, F. Heinrich, J. Bauer, S. Meister, D. Knoll, M. Casalboni, S. Schrader, *IEEE Photonics Technol. Lett.* **2015**, 27, 2197.
- [35] P. Rabiei, W. H. Steier, C. Zhang, L. R. Dalton, *Light. Technol. J.* **2002**, 20, 1968.
- [36] F. Qiu, H. Sato, A. M. Spring, D. Maeda, M. Ozawa, K. Odoi, I. Aoki, A. Otomo, S. Yokoyama, *Appl. Phys. Lett.* **2015**, 107, 123302.
- [37] F. Y. Gardes, A. Brimont, P. Sanchis, G. Rasigade, D. Marris-Morini, L. O'Faolain, F. Dong, J. M. Fedeli, P. Dumon, L. Vivien, T. F. Krauss, G. T. Reed, J. Marti, *2009 6th IEEE Int. Conf. Gr. IV Photonics* **2009**, 17, 241.
- [38] T. Baba, S. Akiyama, M. Imai, N. Hirayama, H. Takahashi, Y. Noguchi, T. Horikawa, T. Usuki, *Opt. Express* **2013**, 21, 11869.
- [39] J.-M. Lee, D.-J. Kim, H. Ahn, S.-H. Park, G. Kim, *J. Light. Technol.* **2007**, 25, 2236.
- [40] M. Lauermaun, R. Palmer, S. Koeber, P. C. Schindler, D. Korn, T. Wahlbrink, J. Bolten, M. Waldow, D. L. Elder, L. R. Dalton, J. Leuthold, W. Freude, C. Koos, *Opt. Express* **2014**, 22, 29927.
- [41] R. Halir, P. J. Bock, P. Cheben, A. Ortega-Moñux, C. Alonso-Ramos, J. H. Schmid, D.-X. Xu, J. G. Wangüemert-Pérez, Í. Molina-Fernández, S. Janz, *Laser Photon. Rev.* **2015**, 9, 25.
- [42] Y. Xiong, D. X. Xu, J. H. Schmid, P. Cheben, W. N. Ye, *IEEE Photonics J.* **2015**, 7, XX.
- [43] J. H. Schmid, P. Cheben, S. Janz, J. Lapointe, E. Post, A. Delâge, A. Densmore, B. Lamontagne, P. Waldron, D. X. Xu, *Adv. Opt. Technol.* **2008**, 17, 19120.
- [44] J. D. Sarmiento-Merenguel, A. Ortega-Moñux, J.-M. Fédéli, J. G. Wangüemert-Pérez, C. Alonso-Ramos, E. Durán-Valdeiglesias, P. Cheben, Í. Molina-Fernández, R. Halir, *Opt. Lett.* **2016**, 41, 3443.
- [45] S. Inoue, A. Otomo, *Appl. Phys. Lett.* **2013**, 103, 171101.
- [46] J. Gonzalo Wangüemert-Pérez, P. Cheben, A. Ortega-Moñux, C. Alonso-Ramos, D. Pérez-Galacho, R. Halir, Í. Molina-Fernández, D.-X. Xu, J. H. Schmid, *Opt. Lett.* **2014**, 39, 4442.
- [47] V. Donzella, J. Flueckiger, A. Sherwali, S. T. Fard, S. M. Grist, L. Chrostowski, *2014 IEEE Photonics Conf. IPC* **2014**, 3, 607.
- [48] P. J. Bock, P. Cheben, J. H. Schmid, J. Lapointe, A. Delâge, S. Janz, G. C. Aers, D.-X. Xu, A. Densmore, T. J. Hall, *Opt. Express* **2010**, 18, 20251.
- [49] J. Flueckiger, S. Schmidt, V. Donzella, A. Sherwali, D. M. Ratner, L. Chrostowski, K. C. Cheung, *Opt. Express* **2016**, 24, 15672.
- [50] X. Xu, H. Subbaraman, J. Covey, D. Kwong, A. Hosseini, R. T. Chen, *Opt. Lett.* **2013**, 38, 3588.
- [51] X. Xu, H. Subbaraman, J. Covey, D. Kwong, A. Hosseini, R. T. Chen, *Appl. Phys. Lett.* **2012**, 101, 31109.
- [52] Z. Wang, X. Xu, D. Fan, Y. Wang, H. Subbaraman, R. T. Chen, *Sci. Rep.* **2016**, 6, 24106.
- [53] X. Xu, Z. Pan, B. Jia, Y. Wang, R. T. Chen, in *Photonics West*, SPIE, **2017**, p. 1010805.
- [54] X. Zhang, A. Hosseini, H. Subbaraman, S. Wang, Q. Zhan, J. Luo, A. K. Y. Jen, R. T. Chen, *J. Light. Technol.* **2014**, 32, 3774.
- [55] L. R. Dalton, *Broadband Opt. Modul. Sci. Technol. Appl.* **2011**, XX, 223.
- [56] G. T. Reed, G. Mashanovich, F. Y. Gardes, D. J. Thomson, *Nat. Photonics* **2010**, 4, 518.
- [57] C. C. Teng, M. A. Mortazavi, G. K. Boudoughian, *Appl. Phys. Lett.* **1995**, 66, 667.
- [58] A. Yacoubian, W. Lin, D. J. Olson, J. H. Bechtel, in *International Symposium on Optical Science and Technology*, Vol. 4455, **2001**, pp. 181.
- [59] H. Chen, B. Chen, D. Huang, D. Jin, J. D. Luo, A. K.-Y. Jen, R. Dinu, *Appl. Phys. Lett.* **2008**, 93, 43507.
- [60] X. Zhang, A. Hosseini, S. Chakravarty, J. Luo, A. K. Y. Jen, R. T. Chen, *Opt. Lett.* **2013**, 38, 4931.
- [61] Ch. Bosshard, K. Sutter, R. Schlessler, P. Gunter, *J. Opt. Soc. Am. B* **1993**, 10, 867.
- [62] Y. Jouane, Y.-C. Chang, D. Zhang, J. Luo, A. K.-Y. Jen, Y. Enami, *Opt. Express* **2014**, 22, 27725.
- [63] L. Chrostowski, M. Hochberg, *Silicon Photonics Design: From Devices to Systems*, Cambridge University Press, **2015**.